Correlated giant dielectric peaks and antiferromagnetic transitions near room temperature in pure and alkali-doped $BaMnO_{3-\delta}$

2011 J. Phys.: Condens. Matter 23 435901

(http://iopscience.iop.org/0953-8984/23/43/435901)

J. Phys.: Condens. Matter **23** (2011) 435901 (8pp) doi:10.1088/0953-8984/23/43/435901

Correlated giant dielectric peaks and antiferromagnetic transitions near room temperature in pure and alkali-doped $BaMnO_{3-\delta}$

O B Korneta[1,2], T F Qi[1,2], M Ge[1,2,3], S Parkin[1,4], L E De Long[1,2], P Schlottmann[5] and G Cao[1,2]

[1] Center for Advanced Materials, University of Kentucky, Lexington, KY 40506, USA
[2] Department of Physics and Astronomy, University of Kentucky, Lexington, KY 40506, USA
[3] Department of Physics, University of Science and Technology of China, Hefei, 230026, People's Republic of China
[4] Department of Chemistry, University of Kentucky, Lexington, KY 40506, USA
[5] Department of Physics, Florida State University, Tallahassee, FL 32306, USA

E-mail: delong@pa.uky.edu and cao@pa.uky.edu

Received 8 June 2011, in final form 1 September 2011
Published 13 October 2011
Online at stacks.iop.org/JPhysCM/23/435901

Abstract

We report structural, magnetic, dielectric and thermal properties of single-crystal $BaMnO_{2.99}$ and its derivatives $BaMn_{0.97}Li_{0.03}O_3$ and $Ba_{0.97}K_{0.03}MnO_3$. The hexagonal 15R-$BaMnO_{2.99}$ perovskite phase is a known antiferromagnetic insulator that orders at a Néel temperature $T_N = 220$ K. We find dilute Li and K doping change the ratio of cubic to hexagonal layers and cause drastic changes in the dielectric and magnetic properties. Unusually large high-temperature magnetoelectric shifts (up to 85%) are observed near temperatures at which pronounced peaks in the dielectric constant are observed for applied electric fields along either the *c* or *a* axis, respectively. The temperatures of the dielectric peaks are strongly correlated with anomalies in the *c*- or *a*-axis magnetic susceptibility and the specific heat for all compositions studied. All our data suggest that the strongly anisotropic magnetic and dielectric anomalies (which occur near, or above room temperature) originate from the same Mn ion sites, which implies these materials form an exceptional class of magnetoelectrics.

(Some figures in this article are in colour only in the electronic version)

1. Introduction

Magnetoelectric (ME) materials are of fundamental and technological interest [1–7] and there is an ongoing quest for new ME materials exhibiting transitions to both (anti)ferroelectric and (anti)ferromagnetic states above room temperature [4–16]. While new materials have emerged in recent years [6–16], remarkably few exhibit coexisting electric and magnetic order at temperatures above 100 K [17–21]. The scarcity of such materials is thought to be due to a fundamental incompatibility between magnetic and electric order; and the prevailing view is that coexistence is more likely to be found in situations where (anti)ferroelectricity and (anti)ferromagnetism originate on different crystallographic sites [6, 21]. In particular, ABO_3 perovskites should not be promising candidates for coexistence, since ferroelectricity is favored when nonmagnetic d^0 transition metal ions occupy the B site [5], which clearly disfavors magnetic order (that requires magnetic ions with partially occupied d-shells) on the same site.

Nevertheless, recent theoretical studies have predicted that a ferroelectric (FE) state driven by the off-centering of magnetic Mn^{4+} (d^3) ions can be established in the cubic perovskite $CaMnO_3$ via strain or chemical manipulation [22],

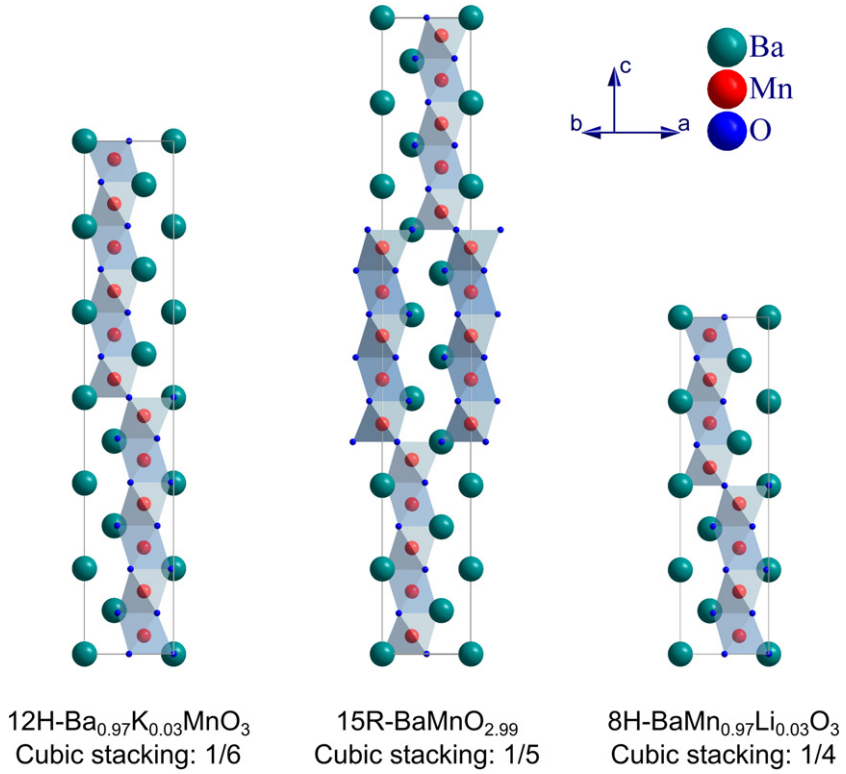

Figure 1. Stacking sequences that define the cubic stacking ratios (CSR) by counting interfaces of a given symmetry between octahedra stacked along the c direction are shown for $Ba_{0.97}K_{0.03}MnO_3$, $BaMnO_{2.99}$ and $BaMn_{0.97}Li_{0.03}O_3$ (from left to right).

and in the hypothetical cubic perovskite $BaMnO_3$ [23]. However, the $BaMnO_3$ phase exists only in the hexagonal perovskite structure because the Goldschmidt tolerance factor is greater than unity (i.e. the ionic radius of the Ba^{2+} ion is too large to accommodate the ideal cubic perovskite structure with $Pm3m$ symmetry). It is important to note that the lattice parameters a, c and V of the ideal cubic (c) and hexagonal (h) perovskite structures of composition ABO_3 are simply related: $a_h = \sqrt{2}a_c$, $c_h = \sqrt{3}a_c$ and $V_h = 3V_c$. Consequently, intermediate structures between the ideal hexagonal and cubic perovskite structures readily form with different proportions of cubic layers (corner-sharing octahedra) and hexagonal layers (face-sharing octahedra). Examples are the $BaMnO_{3-\delta}$ ($\delta < 0.09$) polytypes, in which the ratio of cubic to hexagonal layers, or the cubic stacking ratio (CSR), sensitively depend on the chemical composition and/or oxygen content [24–26] (see figure 1). An easily tuned CSR makes materials based upon $BaMnO_{3-\delta}$ a promising subject for studies of correlations between structural and ME properties. Although the structures of polytypes based on $BaMnO_3$ have been thoroughly investigated [25–31], the physical properties of these materials are not well known, especially compared to those of the cubic and hexagonal manganites $RMnO_3$ (R = Y and heavier rare earths).

Here we report a systematic study of structural, magnetic, dielectric and thermal properties of single-crystal $BaMnO_{2.99}$ and its derivatives $BaMn_{0.97}Li_{0.03}O_3$ and $Ba_{0.97}K_{0.03}MnO_3$, with special attention to the CSR, which assumes the respective values 1/5, 1/4 and 1/6 (see figure 1). We find that these materials have an unusually large, high-temperature ME effect that is accompanied by a more than tenfold enhancement of the dielectric constant $\varepsilon(T)$ near their respective Néel temperatures. The magnetic susceptibility of $BaMnO_{2.99}$ exhibits an unusual anisotropy below T_N, corresponding to a strongly anisotropic maximum in the dielectric response observed near T_N. Dilute Li doping yields an increase of the CSR from 1/5 to 1/4 in the case of $BaMn_{0.97}Li_{0.03}O_3$, accompanied by reduced magnetic anisotropy, lattice softening and a drastic rise in $\varepsilon(T)$ near T_N for an electric field applied along either the a or c axes. The observed correlations between magnetic and dielectric anomalies that occur near or above room temperature comprise strong evidence that the magnetic and dielectric responses arise on the same Mn ion sites, which is an extremely rare combination of phenomena that has important fundamental and technological implications.

2. Experimental details

$BaMnO_{3-\delta}$, $BaMn_{0.97}Li_{0.03}O_3$ and $Ba_{0.97}K_{0.03}MnO_3$ single crystals were grown at ambient pressure using flux techniques [24]. Chemical compositions were determined using energy dispersive x-ray (EDX) analysis. Single-crystal x-ray refinements carried out at both 90 and 295 K using a Nonius-Kappa CCD single-crystal diffractometer (XRD) and the SHELX-97 programs [24]; the results are summarized in tables 1 and 2. Measurements of specific heat $C(T)$ were performed using a Quantum Design PPMS and magnetization $M(T, H)$ for applied magnetic fields $\mu_o H \leq 7$ T

Table 1. Parameters from refinements of single-crystal x-ray data for three representative single crystals at 90 K.

Crystal data			
Chemical formula	$BaMnO_{2.99}$	$BaMn_{0.97}Li_{0.03}O_3$	$Ba_{0.97}K_{0.03}MnO_3$
M_r	240.28	320.37	306.39
Crystal system, space group	Trigonal, $R\bar{3}m$	Hexagonal, $P63/mmc$	Hexagonal, $P63/mmc$
Temperature (K)	90	90	90
a, b, c (Å)	5.6662(8), 5.6662(8), 35.276(7)	5.6619 (8), 5.6619(8), 18.721(4)	5.673(1), 5.673(1), 28.3395(7)
α, β, γ (deg)	90, 90, 120	90, 90, 120	90, 90, 120
V (Å^3)	980.8(3)	519.72(15)	789.9(2)
Z	9	6	6
Radiation type	Mo Kα	Mo Kα	Mo Kα
μ (mm^{-1})	11.72	19.65	11.85
Crystal size (mm)	0.10 × 0.10 × 0.03	0.05 × 0.05 × 0.05	0.05 × 0.05 × 0.05
Data collection			
Diffractometer	Nonius Kappa CCD diffractometer	Nonius Kappa CCD diffractometer	Nonius Kappa CCD diffractometer
Absorption correction	Multi-scan Sadabs	Multi-scan Sadabs	Multi-scan Sadabs
No. of measured, independent and observed [$I > 2\sigma(I)$] reflections	6483, 336, 325	10 795, 276, 254	15 080, 411, 324
R_{int}	0.041	0.038	0.056
Refinement			
$R[F^2 > 2\sigma(F^2)]$, $wR(F^2)$, S	0.017, 0.038, 1.21	0.017, 0.037, 1.30	0.058, 0.170, 1.23
No. of reflections	336	276	411
No. of parameters	34	30	41
No. of restraints	0	0	0
$\Delta\rho_{max}$, $\Delta\rho_{min}$ (e Å^{-3})	2.43, −1.32	1.65, −1.63	5.79, −2.79

using a Quantum Design MPMS. The complex permittivity $\varepsilon(T, H, \omega) = \varepsilon' + i\varepsilon''$ was measured using a QuadTech Model 7600 LCR Meter with a frequency range of 10 Hz $\leq \omega \leq$ 2 MHz in fields $\mu_o H \leq 9$ T, utilizing a custom-built probe for QD PPMS.

3. Results and discussion

3.1. $BaMnO_{3-\delta}$

Single-crystal samples of $BaMnO_{3-\delta}$ were found to adopt the '15R phase' with space group $R\bar{3}m$ (#166) and a CSR = 1/5, as shown in figure 1, which matches the structure previously reported for $BaMnO_{2.99}$ [26]. The compositions $Ba_{0.97}K_{0.03}MnO_3$ and $BaMn_{0.97}Li_{0.03}O_3$ form in the 12H and 8H phases, respectively, with space group $P63/mmc$ (#194); the corresponding CSR = 1/6 for the former and 1/4 for the latter (see figure 1, tables 1 and 2). The refinements for the doped $BaMnO_3$ phases reveal a strong preference for substituted species to locate within the hexagonal layers rather than within the cubic layers [31]. This tendency suggests bonding interactions are relatively strong within the cubic layers, consistent with earlier studies [25, 26, 29]. Moreover, the Mn ions in the cubic and hexagonal layers are asymmetrically positioned within the MnO_6 octahedra, and have a tendency to shift their positions towards the nearest-neighbor cubic layers, resulting in uneven Mn–O and Mn–Mn bond distances [24].

It is expected that all orbital degeneracies are lifted for an Mn^{4+} ($3d^3$) ion in $BaMnO_{2.99}$, and the three orbitals (corresponding to t_{2g} states in cubic symmetry) with lowest energy are half-filled, leading to a spin = 3/2 on each Mn^{4+} site. The basal-plane magnetic susceptibility $\chi_a(T)$ (figure 2(a)) exhibits an anomaly that signals an antiferromagnetic (AFM) state below a Néel temperature $T_N = 220$ K. Remarkably, no anomaly is apparent in the c-axis $\chi_c(T)$, which indicates a strong magnetic anisotropy in $BaMnO_{2.99}$ and suggests that the Mn spins lie within the basal plane below T_N. A planar arrangement of spins is also consistent with a decrease of $\chi_a(T)$ as temperature is reduced in the interval 43 K $\leq T \leq T_N$, whereas $\chi_c(T)$ remains essentially temperature-independent over the same range. Both $\chi_a(T)$ and $\chi_c(T)$ exhibit extremely weak, non-Curie–Weiss temperature dependences for $T > T_N$; in fact, $\chi_a(T)$ increases slightly with increasing temperature, which is unusual. A saw-tooth peak in the specific heat $C(T)$ near 230 K $\approx T_N$ (figure 2(a)) is consistent with a bulk, second-order AFM transition. The isothermal magnetization below T_N exhibits a linear field dependence for applied fields up to 7 T, as expected for an AFM state with $T_N = 220$ K.

Note that impurity phases cannot be responsible for the observed strong anisotropy in anomalies in $\chi_c(T)$, $\chi_a(T)$ and $C(T)$, since impurity signatures in all three properties would generally be visible at very nearly the same temperature. On the other hand, a sharp upturn in both $\chi_a(T)$ and $\chi_c(T)$ observed at $T = 43$ K does not correspond to any clear anomaly in $C(T)$; we will further discuss the 43 K anomalies towards the end of this paper.

One of the central findings in this study is that the higher temperature magnetic anomalies in $BaMnO_{2.99}$ are strongly

Table 2. Atomic position parameters of three representative single crystals at 90 K.

Atom	Ox.	Wyck.	Site	S.O.F.	x/a	y/b	z/c
Atomic parameters for $BaMnO_{2.99}$							
Ba1		3a	−3m		0	0	0
Ba2		6c	3m		0	0	0.133 65(1)
Ba3		6c	3m		0	0	0.265 13(1)
Mn1		3b	−3m		0	0	1/2
Mn2		6c	3m		0	0	0.361 52(3)
Mn3		6c	3m		0	0	0.431 49(3)
O1		9e	.2/m		1/2	0	0
O2		18h	.m		0.1849(3)	−0.1849(3)	0.064 11(8)
O3		18h	.m		0.4840(3)	−0.4840(3)	0.132 76(8)
Atomic parameters for $BaMn_{0.97}Li_{0.03}O_3$							
Ba1		2a	−3m.		0	0	0
Ba2		2b	−6m2		0	0	1/4
Ba3		4f	3m.		1/3	3-Feb	0.128 16(2)
Mn1		4f	3m.		1/3	3-Feb	0.553 51(6)
Mn2		4f	3m.	0.976	1/3	3-Feb	0.685 39(5)
Li2		4f	3m.	0.024	1/3	3-Feb	0.685 39(5)
O1		6g	.2/m.		1/2	0	0
O2		6h	mm2		0.5155(5)	1.031(1)	1/4
O3		12k	.m.		0.8148(3)	1.6296(7)	0.121 14(14)
Atomic parameters for $Ba_{0.97}K_{0.03}MnO_3$							
Ba1		2c	−6m2		1/3	2/3	1/4
Ba2		2a	−3m.		0	1	0
Ba3		4e	3m.		0	1	0.166 89(4)
Ba4		4f	3m.		1/3	2/3	0.084 92(5)
Mn5		4f	3m.		2/3	1/3	0.207 39(10)
Mn6		4f	3m.		−1/3	1.3333	0.035 65(12)
Mn7		4f	3m.		−1/3	1.3333	0.122 27(11)
O1		6h	mm2		0.365(3)	0.1823(16)	1/4
O2		12k	.m.		0.970(2)	0.4848(11)	0.1652(2)
O3		12k	.m.		−0.629(2)	1.1853(11)	0.0800(3)
O4		6g	.2/m.		−1/2	1	0

correlated with anomalies in the dielectric response, as is apparent in figures 2(a) and (b), which exhibit three major features:

(1) The real part of the a-axis dielectric constant $\varepsilon'_a(T)$ is one order of magnitude greater than the c-axis $\varepsilon'_c(T)$ near T_N, which is consistent with spins confined to the basal plane (figure 2(a)).
(2) An applied magnetic field $\mu_o H = 9$ T downshifts a peak in $\varepsilon'_a(T)$ at temperature $T_E \approx 273$ K by 11 K and reduces the peak amplitude by $\Delta\varepsilon'_a(T, H) \equiv [\varepsilon'_a(T_E, 9\ \text{T}) - \varepsilon'_a(T_E, 0)]/\varepsilon'_a(T_E, 0) \approx -13\%$ (figure 2(b)). We also note that $\varepsilon'_c(T)$ exhibits a very weak magnetic field dependence (not shown here).
(3) The magnitude of $\varepsilon'_a(T)$ is surprisingly large near both T_N and T_E and comparable to, or even greater than, values exhibited by well-known magnetoelectrics such as $BaMnF_4$ [2], $BiMnO_3$ [10], $HoMnO_3$ and $YMnO_3$ [13].

Dielectric relaxation is evident in $BaMnO_{2.99}$ at very low frequencies ($f < 50$ kHz), as shown in figure 2(c). Note that a prominent, sharp peak in $\varepsilon'_a(T)$ is located at $T_E = 273$ K for $f = 100$ Hz, is broadened for frequencies both above and below 100 Hz, and also shifts upwards in temperature with increasing frequency. The data of $\varepsilon'_a(T)$ for $f = 20$ Hz is consistent with a Curie–Weiss law for 270 K $< T <$ 365 K and a corresponding fit yields a Curie–Weiss temperature of +257 K (see figure 2(c)), which is intermediate between $T_N =$ 220 K and $T_E = 273$ K. $\varepsilon'_c(T)$ is also frequency-dependent, but exhibits a maximum at higher temperatures (which defines $T_{Ea,c}$ for an electric field along the a or c axis, respectively) and a relatively prominent low-temperature shoulder (figure 2(d)). The frequency dependence of the peak temperature T_E in $\varepsilon'_a(T)$ follows an Arrhenius law, as shown in figure 3, which indicates activated behavior due to an energy gap of the order of 0.45 eV, which is too large an energy to be phononic; therefore it must be electronic in origin. The associated attempt frequency is 10 GHz (i.e. a microwave frequency), which is much smaller than the activation energy.

It is intriguing that the observed frequency dependence of $\varepsilon'(T)$ is typical of a relaxor rather than a ferroelectric;

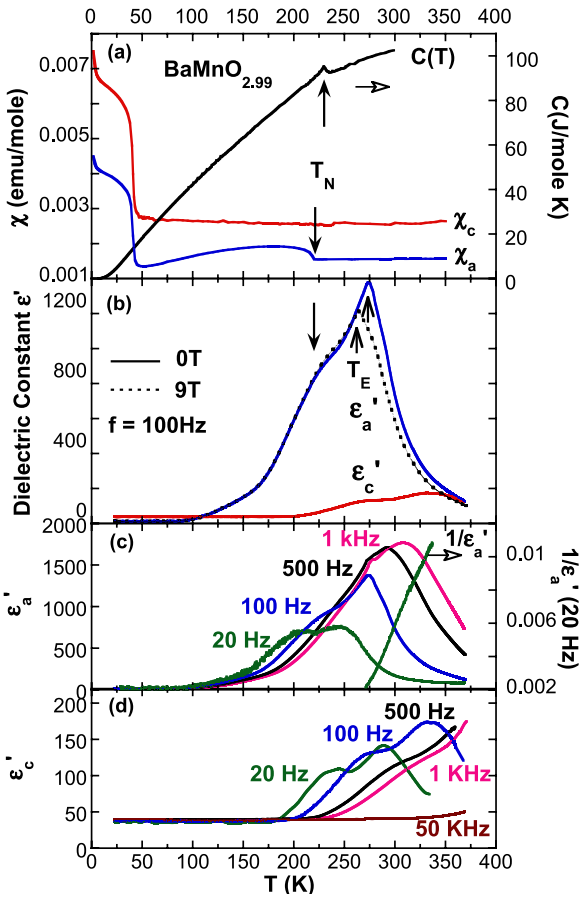

Figure 2. Comparison of specific heat, magnetic and dielectric data for $BaMnO_{2.99}$. (a) Magnetic susceptibility $\chi_a(T)$ for the a axis and $\chi_c(T)$ for the c axis at applied magnetic field $\mu_o H = 0.1$ T and zero-field data for the specific heat $C(T)$ (right scale). Arrows indicate respective values inferred for the Néel temperature T_N. (b) Dielectric constant $\varepsilon'_a(T)$ for electric field along the a axis and $\varepsilon'_c(T)$ for the c axis. The leftmost arrow indicates a shoulder in $\varepsilon'_a(T)$ that corresponds to T_{Na}; the two rightmost arrows indicate values of T_{Ea} inferred from the main peak in $\varepsilon'_a(H, T)$ for $\mu_o H = 0$ (solid blue line) and 9 T (broken black line). (c) $\varepsilon'_a(T)$ at a few representative frequencies and a fit to the Curie–Weiss law $1/\varepsilon'_a(T)$ (right scale). (d) $\varepsilon'_c(T)$ at a few representative frequencies.

but, on the other hand, the Curie–Weiss behavior of $1/\varepsilon'_a(T)$ (figure 2(c)) is characteristic of a typical ferroelectric, but absent in a typical relaxor [34]. In addition, the observed low-frequency dielectric response is remarkably nonlinear near T_E for a given crystal direction and mimics the behavior of certain ferroelectrics such as $AgNa(NO_2)_2$ or $Pb_3MgNb_2O_9$, which are driven by a soft mode whose frequency vanishes at the phase transition [32].

We emphasize that the crystal structure of $BaMnO_3$ is unusually sensitive to slight changes in chemical composition, such as slight variations of oxygen content [26], and Li and K doping (discussed herein). We also observe clear correlations between temperatures of the peaks in the dielectric constants $\varepsilon'_a(T)$ and $\varepsilon'_c(T)$ and anisotropic anomalies (ignoring the jumps near 43 K) in the magnetic susceptibilities $\chi_a(T)$ and $\chi_c(T)$ of $BaMnO_{2.99}$. These observations, coupled with the nonlinear, frequency-dependent relaxor behavior of $\varepsilon'(T)$

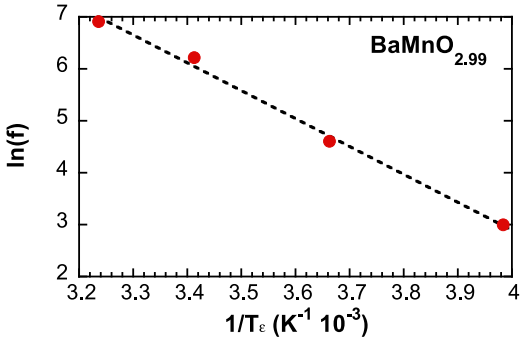

Figure 3. Logarithm of the measuring frequency $\ln(f)$ versus reciprocal peak temperature $1/T_E$ of $\varepsilon'_a(T)$ for $BaMnO_{2.99}$. The dashed line is a guide to the eye demonstrating the activated behavior of $\varepsilon'_a(T)$.

observed near T_N, lead us to hypothesize that the lattice of $BaMnO_{2.99}$ is extraordinarily 'soft' and susceptible to even slight displacements of the Mn ions induced by magnetic ordering and infer that the correlated magnetic and dielectric responses must be attributed to a spin–lattice coupling that displaces the Mn ions relative to the anions when magnetic ordering occurs.

3.2. $BaMn_{0.97}Li_{0.03}O_3$

We now demonstrate how our proposed strong spin–lattice coupling in $BaMnO_{2.99}$ is manifest in the drastic changes in both the magnetic and dielectric behavior induced by a dilute, 3% Li substitution for Mn. It is remarkable that a mere 3% Li doping increases the fraction of cubic layers within the unit cell, raising the CSR from 1/5 to 1/4, as shown in figure 1 and table 1. This structural change generates more pathways along 180° (i.e. cubic stacking) Mn–O–Mn bond angles between the corner-sharing MnO_6 octahedra along the c axis and should be accompanied by a more isotropic magnetic ordering. This expectation is confirmed by our observation of strong anomalies in both $\chi_a(T)$ and $\chi_c(T)$, as shown in figure 4(a); this result is in sharp contrast to the anisotropic magnetic behavior of undoped $BaMnO_{2.99}$, where $\chi_c(T)$ exhibits no discernible magnetic anomaly at T_N (figure 2(a)).

It is intriguing that the robust magnetic anomalies in $\chi_a(T)$ and $\chi_c(T)$ occur at well-separated temperatures: $T_{Na} = 215$ K in the former and $T_{Nc} = 290$ K in the latter susceptibility (figure 4(a); see figure 4(c)). Closer inspection (see a blow-up of the magnetic data in figure 4(c)) reveals a second, broad anomaly in $\chi_a(T)$ with an onset temperature close to the value of $T_{Nc} = 290$ K inferred from the onset of the anomaly in $\chi_c(T)$. Remarkably, $C(T)$ displays a single anomaly at 247 K, approximately midway between T_{Na} and T_{Nc} (see figure 4(a)).

The significant changes we observe in sample behavior with a mere 3% Li doping cannot be explained by sample inhomogeneity or second phases (in which case $C(T)$ should exhibit two peaks corresponding to the well-separated anomalies at T_{Na} and T_{Nc}); neither is there any evidence

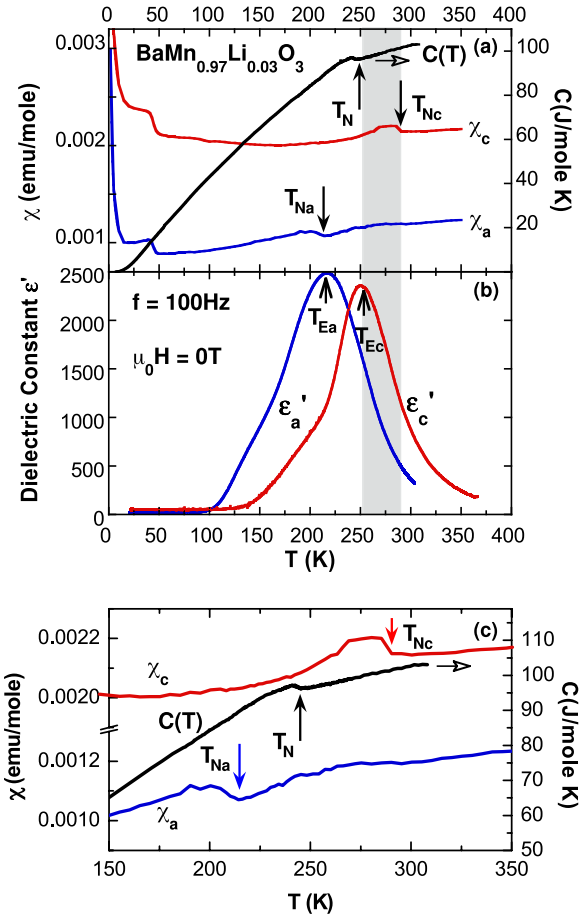

Figure 4. Comparison of specific heat, magnetic and dielectric data for $BaMn_{0.97}Li_{0.03}O_3$. (a) Magnetic susceptibility $\chi_a(T)$ for magnetic field applied along the a axis and $\chi_c(T)$ for the c axis at $\mu_o H = 0.1$ T and specific heat $C(T)$ (right scale). Arrows indicate values of the Néel temperature inferred from respective data. (b) Dielectric constant $\varepsilon'_a(T)$ for electric field along the a axis and $\varepsilon'_c(T)$ for the c axis. Arrows indicate values of the peak temperatures inferred from the respective data. (c) Blow-up of the magnetic and specific heat data of (a) for temperatures near the Néel temperature T_N. In particular, note the broad anomaly in $\chi_c(T)$ with an onset near T_{Na} inferred from $\chi_a(T)$.

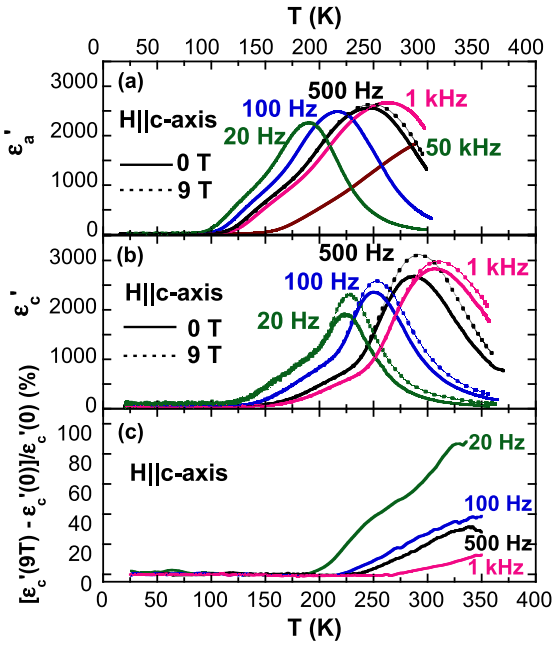

Figure 5. Comparison of the dielectric data measured for magnetic field $H \parallel c$, with electric field along different crystal directions for $BaMn_{0.97}Li_{0.03}O_3$. (a) $\varepsilon'_a(T)$ at a few representative frequencies. (b) $\varepsilon'_c(T)$ at a few representative frequencies at $\mu_o H = 0$ T (solid lines) and 9 T (dashed lines). (c) Magneto-dielectric ratio $[\varepsilon'_c(9\text{ T}) - \varepsilon'_c(0)]/\varepsilon'_c(0)$ (%) versus temperature T.

for extra phases in our single-crystal x-ray refinements. This extraordinary difference in apparent phase transition temperatures defined by either the basal plane or the c-axis data suggests that the spatial alignment of a finite measuring field (1000 Oe) induces an unexpected anisotropy in the higher temperature magnetic response. Alternatively, it is possible that fully three-dimensional spin order (i.e. with well defined order parameters in both the a and c directions) is achieved via at least two distinct phase transitions in the higher temperature regime, 250 ± 40 K, which is consistent with the identification of the second, broad anomaly in $\chi_c(T)$ shown in figure 4(c).

In spite of the complicated magnetic anisotropy revealed in figures 2 and 4, an overriding, important result is that the peak temperatures in $\varepsilon'_a(T)$ and $\varepsilon'_c(T)$ closely follow the observed anomalies in $\chi_a(T)$ and $\chi_c(T)$. We note peaks at $T_{Ea} \approx T_{Na} = 215$ K for the a-axis data and at $T_{Ec} = 250$ K $\approx T_{Nc} = 290$ K for the c-axis data, (see the shaded areas in figure 4). Moreover, the dielectric properties are extremely sensitive to dilute substitution of Li for Mn; in particular, the magnitude of $\varepsilon'_c(T)$ for $BaMn_{0.97}Li_{0.03}O_3$ at $T \approx T_{Ec} = 250$ K is more than one order of magnitude greater than that for $BaMnO_{2.99}$ at $T_E = 273$ K. This radical enhancement in $\varepsilon'_c(T)$ suggests a lattice softening occurs at T_E and that the increase in the $\varepsilon'_c(T)$ peak correlates with a reduced magnetic anisotropy and increased CSR in Li-doped samples. One possibility is that Li doping causes a 'critical slowing' of the dielectric fluctuations (relaxor behavior) near T_E and T_N without introducing larger-scale structural disorder that might be expected with larger (e.g. 10%) doping levels. The inferred, strong spin–lattice coupling is further corroborated by the magnetic field shifts of both $\varepsilon'_a(T, H)$ and $\varepsilon'_c(T, H)$, with the latter having a stronger field dependence (see figure 5). The resulting frequency-dependent magneto-dielectric shift (defined as $[\varepsilon'_c(9\text{ T}) - \varepsilon'_c(0)]/\varepsilon'_c(0)(\%)$), rises from +20% for $f = 1$ kHz to near +85% for $f = 20$ Hz near T_N (see figure 5(c)).

3.3. $Ba_{0.97}K_{0.03}MnO_3$

The marked differences in magneto-dielectric behavior between $BaMn_{0.97}Li_{0.03}O_3$ and $BaMnO_{2.99}$ demonstrate that a modest 3% Li doping has a substantial impact on a spin–lattice coupling that we propose must accompany an increased CSR and lower anisotropy. The validity and importance of this proposal can be checked: it is necessary that the doping effects be reversed when the CSR is reduced, as we indeed have verified in data for $Ba_{0.97}K_{0.03}MnO_3$,

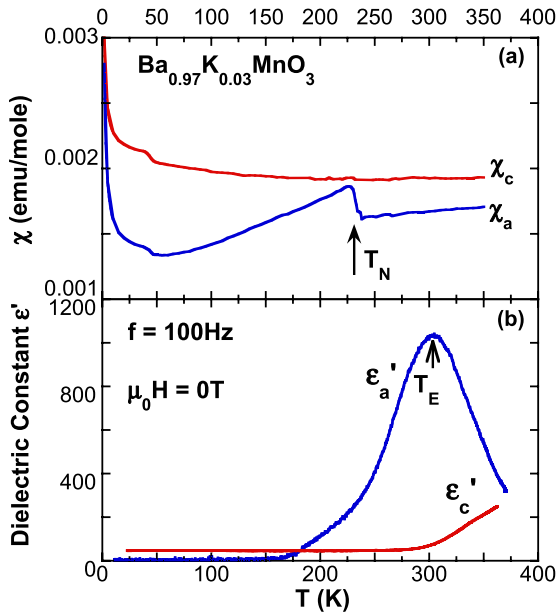

Figure 6. Comparison of the dielectric and magnetic data for $Ba_{0.97}K_{0.03}MnO_3$. (a) Magnetic susceptibility $\chi_a(T)$ for field along the a axis and $\chi_c(T)$ for the c axis at $\mu_o H = 0.1$ T. The arrow indicates the inferred value of the Néel temperature T_N. (b) Dielectric constant $\varepsilon'_a(T)$ for electric field along the a axis and $\varepsilon'_c(T)$ for the c axis at frequency $f = 100$ Hz. The arrow indicates the inferred value of the peak temperature T_E inferred from the a-axis data.

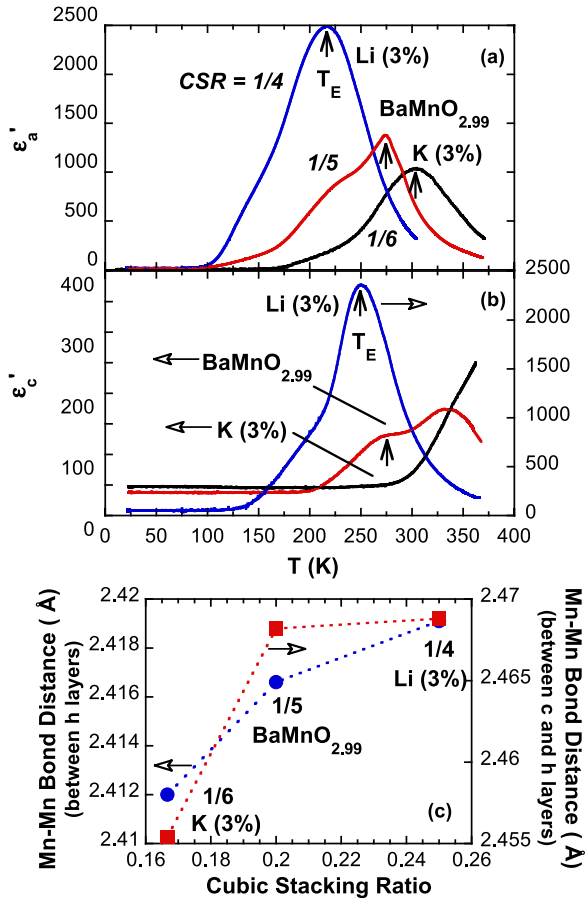

Figure 7. Comparisons of (a) $\varepsilon'_a(T)$ and (b) $\varepsilon'_c(T)$ measured at frequency $f = 100$ Hz. Arrows indicate the values of the peak temperatures T_E inferred from the data. (c) Mn–Mn bond distances between hexagonal layers (left scale) and between cubic and hexagonal layers (right scale) as a function of the cubic stacking ratio for $BaMnO_{2.99}$, $BaMn_{0.97}Li_{0.03}O_3$ and $Ba_{0.97}K_{0.03}MnO_3$.

for which the CSR is reduced from 1/5 for $BaMnO_{2.99}$ to 1/6 with only a 3% K doping (figure 1 and table 1). As shown in figure 6(a), an anomaly in $\chi_a(T)$ signals magnetic ordering at $T_N = 230$ K, whereas no corresponding anomaly is discerned in $\chi_c(T)$ (similar to the case of $BaMnO_{2.99}$ in figure 2(a)), which is indicative of a stronger magnetic anisotropy due to a weakened superexchange interaction along the c axis. This stronger magnetic anisotropy, in turn, leads to a weaker dielectric response (see figure 6(b)). On the other hand, $\varepsilon'_a(T)$ peaks at a much higher temperature than any other anomaly that we have observed and $\varepsilon'_c(T)$ appears to peak at still higher temperature. We investigated the magnetic field shift of $\varepsilon'_c(T, H)$, which is expected to have a stronger field dependence than $\varepsilon'_a(T, H)$ (based upon the $BaMn_{0.97}Li_{0.03}O_3$ data in figure 5), for temperatures below 360 K and frequencies $f = 100$ and 500 Hz. However, the frequency-dependent magneto-dielectric shift $\Delta\varepsilon'_c(9\text{ T}, T) = [\varepsilon'_c(9\text{ T}, T) - \varepsilon'_c(0, T)]/\varepsilon'_c(0, T)$ was immeasurably small for each frequency (which is expected, since $T \leq 360$ K does not include the anticipated field-sensitive region on the high-temperature side of the peak in $\varepsilon_c(0, T)$, as is the case in figure 5(b)). Additional higher temperature dielectric measurements are needed to clarify the behavior of $Ba_{0.97}K_{0.03}MnO_3$.

4. Conclusion

The correlated anomalies in the magnetic susceptibility and the dielectric constant in these materials clearly reveal that the dielectric response is strongly linked to the AFM order; we suspect this linkage causes displacements of the Mn ions via strong spin–lattice coupling, which is accompanied by phonon softening. Such displacements could be very subtle, but other work suggests they could be sufficient to trigger an anomalous dielectric response or a phase transition [33]. Figure 7 illustrates a comparison of $\varepsilon'_a(T)$ and $\varepsilon'_c(T)$ for all three compounds studied and shows that the dielectric response is enhanced by increasing cubic stacking ratio.

Our results appear consistent with a recent first-principles density-functional calculation that predicts a ferroelectric ground state in a hypothetical cubic perovskite $BaMnO_3$ [23]. The t_{2g} and e_g states of the magnetic Mn^{4+} ions are found to be strongly hybridized with the O 2p orbitals, which shifts a delicate balance between competing energies governing the second-order Jahn–Teller effect that favors off-centering and an FE instability. The second-order Jahn–Teller effect is also associated with the relaxation of the electronic system and anomalously large Born effective charges (larger than the formal charges on the ions) in response to the ionic displacements generated through covalent bond formation. Anomalously large Born effective charges are therefore

consistent with off-centering distortions or an FE instability that is signaled by a large dielectric constant. Therefore, our observation of a large dielectric constant that obeys a Curie–Weiss law in undoped $BaMnO_{3-\delta}$and increases with increasing CSR in doped $BaMnO_{3-\delta}$ suggests a proximity to an FE instability. A close examination of the crystal structures of all three compositions under study demonstrate that the Mn–Mn bond distances between hexagonal layers and between cubic and hexagonal layers increase systematically with CSR (see figure 7(c)). We observe that this increased Mn–Mn bond distance is accompanied by weaker magnetic anisotropy that relaxes the lattice via spin–lattice coupling and parallel increases in both $\varepsilon'_a(T)$ and $\varepsilon'_c(T)$ that eventually exceed 2200 near T_N for $BaMn_{0.97}Li_{0.03}O_3$ (see figures 4 and 7).

Finally, we address lower temperature steps in both $\chi_a(T)$ and $\chi_c(T)$ data which are apparent near $T = 43$ K for $BaMnO_{3-\delta}$ and lightly Li- and K-doped $BaMnO_{3-\delta}$ (see figures 2(a), 4(a) and 6(a)), which indicates the possible presence of a common impurity phase included in our single crystals. Recent magnetic and thermal data [35] indicate that these anomalies are consistent with the presence of order 0.01% or less molar concentration of Mn_3O_4, which undergoes several closely spaced magnetic transitions near 43 K. We would not expect such a small concentration of inclusions to affect our bulk heat capacity data near 43 K to any substantial degree, which is consistent with the specific heat data in figures 2(a) and 4(a). More importantly, the possible existence of such inclusions does not compromise our main conclusions regarding the striking correlations between the higher temperature magnetic and dielectric anomalies that we have emphasized above.

In summary, $BaMnO_{3-\delta}$ and lightly Li- and K-doped $BaMnO_{3-\delta}$ exhibit strong magnetoelectric effects near room temperature. Strong anomalies in the dielectric constants of these materials, comparable to those of well-known ferroelectrics, are closely associated with magnetic ordering temperatures and magnetic anisotropy that sensitively depends on the cubic stacking ratio. The strong correlation between the high-temperature magnetic and dielectric anomalies strongly indicates that they originate on the same Mn ion sites, a highly unusual circumstance that should be checked in future investigations of this group of materials. The proximity of the magnetic and dielectric anomalies to room temperature also makes these materials potentially important for technological applications.

Acknowledgments

This work was supported by NSF through grants DMR-0552267 and DMR-0856234 (GC) and EPS-0814194 (GC, LED) and by DoE through grants DE-FG02-97ER45653 (LED) and DE-FG02-98ER45707 (PS).

References

[1] Ascher E, Rieder H, Schmid H and Stossel H 1966 *J. Appl. Phys.* **37** 1404–5
[2] Scott J F 1977 *Phys. Rev.* B **16** 2329–31
[3] Schmid H 1994 *Proc. 2nd Int. Conf. on Magnetoelectric Interaction Phenomena in Crystals* vol 162 (London: Taylor and Francis) pp 317–38
[4] Eerenstein W, Mathur N D and Scott J F 2006 *Nature* **442** 759–65
[5] Spaldin N A, Cheong S-W and Ramesh R 2010 Multiferroics: past, present and future *Phys. Today* **63** 38–43
[6] Khomskii D 2006 *J. Magn. Magn. Mater.* **306** 1–8
[7] Hill N A 2000 *J. Phys. Chem.* B **104** 6694–709
[8] Filippetti A and Hill N A 2001 *J. Magn. Magn. Mater.* **236** 176–89
[9] Fiebig M, Lottermoser T, Frohlich D, Goltsev A V and Pisarev R V 2002 *Nature* **419** 818–20
[10] Kimura T, Kawamoto S, Yamada I, Azuma M, Takano M and Tokura Y 2003 *Phys. Rev.* B **67** 180401
[11] Kimura T, Goto T, Shintani H, Ishizaka K, Arima T and Tokura Y 2003 *Nature* **426** 55–8
[12] Van Aken B B, Palstra T T M, Filippetti A and Spaldin N A 2004 *Nature Mater.* **3** 164–70
[13] Lorenz B, Wang Y Q, Sun Y Y and Chu C W 2004 *Phys. Rev.* B **70** 212412
[14] Lorenz B, Litvinchuk A P, Gospodinov M M and Chu C W 2004 *Phys. Rev. Lett.* **92** 087204
[15] Hur N, Park S, Sharma P A, Ahn J S, Guha S and Cheong S-W 2004 *Nature* **429** 392–5
[16] Ranjith R, Kundu A K, Filippi M, Kundys B, Prellier W, Raveau B, Laverdiére J, Singh M P and Jandl S 2008 *Appl. Phys. Lett.* **92** 062909
[17] Cao G, O'Reilly J W, Crow J E and Testardi L R 1993 *Phys. Rev.* B **47** 11510–1
[18] Fiebig M 2005 *J. Phys.* D **38** R123
[19] Huang Z J, Cao Y, Sun Y Y, Xue Y Y and Chu C W 1997 *Phys. Rev.* B **56** 2623–6
[20] Lonkai T, Tomuta D G, Amann U, Ihringer J, Hendrikx R W A, Tobbens D M and Mydosh J A 2004 *Phys. Rev.* B **69** 134108
[21] Ramesh R and Spaldin N A 2007 *Nature Mater.* **6** 21–9
[22] Bhattacharjee S, Bousquet E and Ghosez P 2009 *Phys. Rev. Lett.* **102** 117602
[23] Rondinelli J M, Eidelson A S and Spaldin N A 2009 *Phys. Rev.* B **79** 205119
[24] Qi T F, Parkin S and Cao G 2011 private communication
[25] Negas T and Roth R S 1971 *J. Solid State Chem.* **3** 323–39
[26] Adkin J J and Hayward M A 2007 *Chem. Mater.* **19** 755–62
[27] Katz L and Ward R 1964 *Inorg. Chem.* **3** 205–11
[28] Chamberland B L, Sleight A W and Weiher J F 1970 *J. Solid State Chem.* **1** 512–4
[29] Jacobson A J and Horrox A J 1976 *Acta Crystallogr.* B **32** 1003–8
[30] Cussen E J and Battle P D 2000 *Chem. Mater.* **12** 831–8
[31] Adkin J J and Hayward M A 2006 *J. Solid State Chem.* **179** 70–6
[32] Lines M E and Glass A M 1977 *Principles and Applications of Ferroelectrics and Related Materials* (Oxford: Clarendon) p 140, 286, 393
[33] Frohlich D, Leute St, Pavlov V V and Pisarev R V 1998 *Phys. Rev. Lett.* **81** 3239–42
[34] Samara G 2001 *Solid State Physics* vol 56, ed H Ehrenreich and F Spaepen (New York: Academic) p 270
[35] Guillou F, Thota S, Prellier W, Kumar J and Hardy V 2011 *Phys. Rev.* B **83** 094423